Geosynthetic reinforcement of pile-supported embankments

Romain Girout, Matthieu Blanc, Luc Thorel, Daniel Dias

Geosynthetic reinforcement of pile-supported embankments

Author(s): Romain Girout[1*], Matthieu Blanc[2], Luc Thorel[3] and Daniel Dias[4]

[1] Post-doctoral Researcher, Department of Civil and Environmental Engineering, COPPE, Federal University of Rio de Janeiro, Ilha do Fundão, RJ 21945-970, Brazil.

E-mail: rgirout@gmail.com (corresponding author)

[2] Researcher, IFSTTAR, Department GERS, Laboratory Geomaterials and Models in Geotechnics, Route de Bouaye, Point 86, CS4, 44344 Bouguenais Cedex, France.

E-mail: matthieu.blanc@ifsttar.fr

[3] Senior Researcher, IFSTTAR, Department GERS, Laboratory Geomaterials and Models in Geotechnics, Route de Bouaye, Point 86, CS4, 44344 Bouguenais Cedex, France.

E-mail: luc.thorel@ifsttar.fr

[4] Professor, Grenoble Alpes University, 3SR Laboratory, 3SR Lab, UMR 5521, BP53, 38041 Grenoble Cedex 09, France,

E-mail: daniel.dias@3sr-grenoble.fr

Geosynthetics international, ICE Publishing Ltd, 25, 1 (2018), pp. 37-49
https://doi.org/10.1680/jgein.17.00032

ABSTRACT

Rigid piles are used to reinforce soft soil base and increase embankment stability. This technique is improved by placing one or more geosynthetic reinforcement (GR) layers inside or at the base of the embankment. A series of 33 small scale models has been tested using a geotechnical centrifuge. Soft soil settlement is imposed by the downward displacement of a tray. First, a series of models is prepared to examine how the load transmitted to the pile network increases with the embankment thickness. For a same configuration, two identical models are prepared to test successively two different types of GR (Geosynthetic Reinforcement). Another approach consists in studying how the external surcharges applied on the embankment affect load transfer. The results show that, in comparison with the piled embankment, the load transfer is increased in the case of the Geosynthetic-Reinforced Pile-Supported Embankment (GRPSE) due to the membrane effect. The membrane effect is higher when the GR is stiff and its vertical distance from the pile is reduced. Numerical modelling reveals that, when adding a GR layer, the second GR has an effect only if punching is sufficient. However, the benefits of it could not be highlighted here.

Key-words: Geosynthetics, piles, embankment, arching, membrane effect

1. INTRODUCTION

One technique for the safe building of embankments on soft to very soft soils consists in driving a network of rigid piles into the soft soil until they reach harder surfaces. Part of the load is transferred within the embankment towards the piles through shearing and arching effects.

In order to enhance the efficiency of this composite foundation, a Geosynthetic Reinforcement (GR) can be added (Fig. 1a). The deformation of the GR acts as a horizontal reinforcement through membrane effect (Villard and Giraud, 1998). The presence of the GR within the embankments also allows for the reduction of the post-construction final settlements. To this day, Geosynthetic-Reinforced Pile-Supported Embankment (GRPSE) is a technique, which is studied using field or full-scale experimental cases (Le Hello, 2007; Briançon and Simon, 2012; Briançon and Dias, 2015 ; Nunez et al., 2013 ; Xing et al., 2014 ; Chen et al., 2016), 1×g small-scale models at a scale of 1/N (Jenck et al., 2005, Jenck et al., 2007, Eskişar et al., 2012, Van Eekelen et al. (2012a, b, 2015)) and centrifuge modelling at a scale1/N and a g-level equals to N (Ellis and Aslam, 2009; Blanc et al., 2013; Girout et al., 2014). These physical modelling tests have been often supplemented by numerical analyses (Le Hello and Villard, 2009; Girout et al., 2014 or Han-Jiang et al., 2014; Zhuang and Ellis, 2016; Zhuang and Wang, 2015; 2016) .

Some standard and design guidelines like EBGEO (2011) have been examined by Blanc et al. (2014), for which the vertical displacement of a GR strip between two piles is compared with the physical modelling results. Girout et al. (2016) have carried out this comparison in the case of unreinforced piled embankment. Van Eekelen et al. (2015) have validated their concentric arching model through a comparison between seven field tests and four small scale models. A recent analytical computation (not compared in the present study) proposed by King et al. (2017) demonstrates the need for some models coupling arching and stress-deformation to describe embankment behaviour reliably.

Different in-situ studies have been conducted to carry out a comparison between piled-embankment and GRPSE, including a multi-layer GRPSE (Bhasi and Rajagopal; 2014; Briançon and Simon, 2017) to examine load transfer toward the piles, settlement and GR deformation.

Okyay et al. (2014) and Fagundes et al. (2015) have conducted their tests using the Mobile Tray (MT) presented in Fig. 2. This device principle consists in simulating, through the tray displacement, the settlement due to the compressibility of the soft soil instead of modelling

soft soil. Using the same MT device, Blanc et al. (2013) have carried out tests on thin granular embankments, with a surcharge applied on the surface in order to examine GR improvement (Fig. 1b). As a conclusion of this study, it appears that a pre-tension applied to the GR does not increase significantly load transfer toward the piles. The same observation is made for the tests conducted with two layers of GR instead of one. This research has also led to the conclusion that the stiffer the GR is, the lower the final deformation of the GR. The embankment thickness never exceeds more than 1.8m. Only one secant stiffness is tested for the geosynthetic reinforcement. The hydraulic load is kept constant and the geosynthetic reinforcement is placed below the embankment. Girout et al. (2016) and Fagundes et al. (2015) have used the MT device only for unreinforced piled embankment studies (e.g., without GR) and performed many tests to investigate embankment behaviour by varying the characteristics of the piled-embankment (thickness H, spacing s between the piles axis, and pile diameter d). The measurements obtained from the load sensors, placed inside the piles at the network center and used to obtain the mean load $F_{m,}$ have been analyzed using the load transfer efficiency equation (Hewlett and Randolph, 1988) as:

$$E_F = \frac{F_m}{\left(\rho_d \cdot g \cdot N \cdot H + q_0\right) \cdot s^2} \quad (1)$$

where F_m is the average load measured per pile unit, $\rho_d \cdot g \cdot N \cdot H$ is the vertical stress due to the embankment thickness with ρ_d the embankment density, g the earth acceleration and N the scale of model, q_0 is the additional homogeneous stress resulting from the hydraulic load applied on the embankment surface with a membrane that separates the water from the soil. The nine load sensors are placed on the inside of the top of the piles. For a piled embankment, this measurement corresponds to the arching effect (called A in the literature). For a GRPSE, it corresponds to the sum $A + B$, where B is the load transferred by membrane effect. Considering the difficulty of calibrating total stress cells dealing with scaling law issues in small-scale model samples, it was not possible to install load cells inside the embankment above the geosynthetic reinforcement to measure B separately. For this reason, the results are analyzed considering the efficiency E_F.

The aim of this paper is to present the findings of the experimental investigation carried out to examine the GR layer (s) reinforcement of a piled-embankment using the MT device. The spacing and the pile diameter are kept constant and are equal to 2.0 m and 0.5m, respectively. First, some tests are conducted to examine the load transfer as a function of the embankment thickness for unreinforced and reinforced piled-embankments. These investigations are

carried out by considering the geosynthetic reinforcement with different secant stiffness values (4.0 MN/m and 16.8 MN/m). Then, the impact on the arching effect of the distance between the piled embankment basal and the horizontal GR is studied through a series of tests conducted on a 7.2-m thick embankment by increasing the GR elevation within the embankment. Finally, the results of the tests carried out with the same initial load on the mobile tray, though applied differently (by using water tank or embankment thickness), are compared in terms of efficiency.

2. PHYSICAL MODELLING IN GEOTECHNICS

By increasing artificially the standard earth gravity, g, by a factor N, centrifuge modelling makes it possible to study a $1/N$ small scale model using the same stress and deformation levels than a full scale prototype (Garnier et al., 2007). In this study, N is equal to 20. Table 1 presents the different scaling factors linking both model and corresponding prototype. The scale factors for the geosynthetic secant stiffness and the length here are equal to $1/N$.

3. EXPERIMENTAL DEVICE

3.1.1. *Description*

The Mobile Tray method, used by Blanc et al. (2013) for the investigation of GR insertions, consists in imposing some displacements $\Delta\omega$ to a perforated steel tray above a rigid pile network to simulate soft soil settlement (Fig. 2a). A model embankment is installed on the tray using a varying number of steel rings depending on the chosen thicknesses (Fig. 2b). The embankment sand material is poured manually until the desired total height is reached and the density is ρ_d = 1.62 kg/m^3. The pile network and the granular embankment main characteristics (spacing and thickness) can be modified. Depending on the tests, one or two GR layers are optionally inserted beneath the model embankment on the MT surface. A surcharge can also be applied on the embankment top surface using a tank filled with water. The tank bottom is made of a soft membrane resting on the top of the embankment (Blanc et al., 2013).

3.1.2. *Materials*

The embankment is made of a mix of five Hostun sand fractions used to model the full scale gravel (Girout et al., 2014). In order to avoid scale effects, the mix is cut at 1 mm (the pile diameter considered here being equal to 25mm). The characteristics of the Hostun sand mix are summarized in Table 2.

As the secant stiffness for the small scale GR has to be N times lower than the prototype, a woven polypropylene geosynthetic has been selected to simulate prototype geogrids. The GR is characterized by the stiffness in the machine direction (i.e., the direction in paper and board that coincides with the longitudinal direction of the web) and the stiffness in the cross machine direction (direction perpendicular to the machine direction). The characteristic values (T_{max} and ε_{max}, which are the maximum tensile load and deformation, respectively) are presented in Table 3 for PP25 and PP60 materials. As an illustration, PP25 basal GR results are displayed in Fig. 3. The test begins when the MT is placed into the swinging basket of the

centrifuge. The entire process is described in Blanc et al. (2013) as regards the tests including a surcharge, for which the water tank is filled until the expected stress level is reached. The tests conducted without surcharge are quicker because the tank does not need to be filled with water. Then, the test procedure only consists in prescribing a displacement $\Delta\omega$ to the tray up to 30mm (i.e., a soft soil displacement equal to 600 mm on prototype scale).

3.1.3. *Experimental campaign*

In situ, the pile network is designed by the ratio of the pile area $\pi.d^2/4$ to the mesh area s^2 (for a square pattern), called the area replacement ratio, α. The tests are conducted for one single area replacement ratio: α = 4.91 % and four thicknesses: H = 1.8 m, 3.2 m, 5.0 m and 7.2 m on prototype scale. In order to establish the relationship between H, s and d, the authors use the parameter $H_{arch,}$ defined as half the length of the diagonal between the pile edges as described by:

$$H_{arch}=\left(s\sqrt{2}-d\right)\Big/2 \tag{2}$$

The tests and their characteristics are presented in Table 4. The tests written in bold (17 tests) have already been published in Fagundes et al. (2017), Girout et al. (2014) or Girout et al. (2016). Initially developed during the French national project A.S.I.Ri (IREX, 2012), the MT device is used to investigate load transfer towards rigid inclusions either within embankments toward the rigid piles, into granular mattresses below a slab or into lime and cement treated soils (Okyay, 2010; Okyay and Dias, 2010). To this a GR material can be added (Blanc et al., 2014). The influence of the different types of surcharge loads on the stress applied on the mobile tray surface is investigated. As illustrated in Fig. 4, different configurations can be used to obtain the same initial stress applied on the tray. Considering ρ_d = 1.62 kg/m^3, the initial stress applied on the GR is equal to the sum of the hydraulic column and the granular column, i.e., 80kPa + 1.62·9.81·1.8 = 109 kPa, to which the weight of the soft membrane (4 kPa) must be added (Okyay et al., 2010). We then obtain 113kPa. As a comparison, the stress induced by a 7.2-m high embankment (T10 and T17 test models) is 114kPa.

4. TESTS ANALYSIS

The test series is conducted to examine how a GR insertion influences piled embankment behaviour for different thicknesses H and surcharges q_0. With this aim in view, different types of models are prepared: with basal GR (i.e., at the soft soil/embankment interface) and without GR. Two different GR stiffness values are tested, characterized by their secant stiffness J_a: first, J_a = 4.0 MN/m and then, J_a = 16.8 MN/m.

The efficiency E_F is plotted as a function of $\Delta\omega$, of H (Fig. 5, Fig. 7a, Fig. 8a, b and Fig. 9) and of h_{gx}/H (Fig. 7b), where h_{gx} is the elevation of the GR within the embankment. In order to address the influence of the thickness, the efficiency is compared as a function of H for different $\Delta\omega$ (0.02, 0.08 and 0.56m) in Fig. 5b. We consider both non-reinforced and geosynthetic-reinforced pile-supported embankments. The displacement values are chosen in order to compare efficiency values ranging from very small displacements (just before the maximum efficiency is reached), to maximum displacement values imposed to the tray. When the efficiency reaches its maximum value, the particular value of the tray displacement is plotted as a function of the embankment thickness (Fig. 5b). For the reinforced case, this corresponds to the vertical displacement δ_g of the GR at the center of the mesh.

4.1. *Unreinforced piled embankments*

The load transfer efficiency versus embankment thickness is first investigated for four different thickness values (H= 1.8m, 3.2m, 5.0m and 7.2m, respectively). First, no surcharge is considered (i.e., q_0 = 0 kPa).

Considering the curves $E_F - \Delta\omega$ in Fig. 5a for the unreinforced piled embankment model (tests T1-4-7 and 10, No GR), the efficiency increases with the tray displacement. All the curves are asymptotic save for the case H = 1.8m. The maximum value reached by the efficiency E_F clearly increases with the thickness. However, for large tray displacements ($\Delta\omega$ = 0.56m), the efficiency for a thin embankment (H = 1.8m) decreases up to its initial value. This behaviour is similar to that of the stress deviator for a dense sample in triaxial tests. In other words, the decrease of the efficiency only is due to the high displacement induced by the tray. As regards in-situ embankments, settlement is lower and results from the stress applied on its surface. The difference in results between the test in the case H = 1.8 m and the other tests is due only to the fact that it is not possible to impose sufficient displacement.

Fig. 5b presents the comparison for the same tray displacement levels: low (0.02m), medium and high (0.56m). The curves with the circular marker (case No GR) show that when the

195 thickness is low (H = 1.8m), the efficiency is less dependent upon soft soil settlement
196 because, contrary to thick embankments (H = 7.2m), the arching effect is low.
197 Fig. 5 (case No GR), on the other hand, displays the tray displacement values when the
198 efficiency reaches its maximum (i.e., $E_F = E_{Fmax}$). The curves increase linearly up to an
199 embankment thickness equal to 5 m and then plateau for the higher thicknesses studied.
200 Considering that the efficiency reaches a maximum value (approximately 65% for H = 7.2m
201 and α = 4.91%) and that it increases with the tray displacement, it is consistent that the
202 settlement itself reaches a maximum value. In other words, above a certain thickness (related
203 to the area replacement ratio), the efficiency does not increase any more. Because of a lower
204 total embankment weight, the thinner the embankment, the smaller the displacement required
205 to reach the maximum efficiency.
206 It can, therefore, be concluded that the load transfer efficiency increases with the embankment
207 thickness by arching effect. In the modelling study presented here, it reaches 65% for H =
208 7.2m (with α = 4.91%). The arching effect occurs with the prescribed displacement (i.e., soft
209 soil displacement) whereas settlement increases with embankment thickness.
210

4.2.*Geosynthetic-Reinforced Pile-Supported Embankments*

The aim of this section is to investigate how the GR decreases the stress applied on soft soil with relation to embankment thickness and GR stiffness. The same models as those already used are then reinforced with a basal horizontal GR. We first examine how the secant stiffness of the GR layer affects load transfer. Two different GR stiffness values are tested (4.0 MN/m and 16.8 MN/m, respectively). According to Fig. 5a, in which the efficiency versus the tray displacement is plotted for the 4.0 MN/m stiff GR, the efficiency increases because of the membrane effect when the soft soil settlement is high enough. For very small displacements ($\Delta\omega$ < 0.05m), unreinforced and 4.0-MN/m stiff GR reinforced embankments are very close (Fig. 5b), even equal for thick embankments. This may be accounted for by the fact that the GR must be subjected to stress to "act" and because the stress applied on the soft soil in the case of thick embankments is higher (i.e., in case of lower efficiency). The lower the tray, the higher the GR is in tension (Fig. 3). For larger displacements ($\Delta\omega$ > 0.23m), the efficiency reaches 100% whatever the thicknesses considered.

In the present case, it is possible to lower the tray until the GR loses its contact with the tray ($\delta_g = \Delta\omega$ for E_F = 100%). This point is equivalent to the conservative case used in standards to design GR, for which the soft soil strength is not taken into account to calculate the stability of this composite foundation.

Fig. 6 displays a comparison of the tray displacements, for which the efficiency is highest ($\Delta\omega_{max} = \Delta\omega$ red on the y-axis to the left when unreinforced piled embankments are considered) with the case, for which the GR displacement is at its maximum (case GR, corresponding to the point where E_F reaches its maximum value). Fig. 6 shows that δ_g (GR deflection, red on the y-axis to the right) increases with the stress applied on the tray (i.e., the embankment thickness) whatever the thickness studied. The load transferred inside the embankment by shearing effect increases with the embankment thickness. The difference between this particular value $\Delta\omega$ and the deflection value δ_g increases with the thickness until full arching effect occurs. Regarding thin non-reinforced embankments, the GR supports fewer loads and its maximum deformation is nearly reached when the maximum efficiency is obtained. Fig. 6 presents the results for both GR stiffness values (4.0 MN/m and stiffer 16.8 MN/m). The slope of the trend line for J_a = 4.0 MN/m is approximately twice that for J_a = 16.8 MN/m. This can be accounted for by the fact that the GR is tensioned according to its stiffness and to the load applied on its surface. As a result, the deflection of the geosynthetic

depends mainly on the load applied on the geosynthetic, therefore on the thickness H and consequently also on its stiffness.

The interesting finding of this work is the fact that, with a GRPSE, the membrane effect permits the improvement of the total load transfer toward the piles. The stiffer the geosynthetic is, the lower the deflection.

4.3.*Elevation of geosynthetic layers within the embankment*

Commonly, piled-embankments are reinforced using a geosynthetic layer placed close to the embankment/soft soil interface. As recommended by the EBGEO design guide (2011) in order to prevent the stress concentration at the pile cap corner from damaging the GR, a thin granular layer can be laid between GR and soft soil, as was also implemented on an experimental in situ embankment (Briançon and Simon, 2017). The aim of this section is to examine how the load transfer efficiency depends on the thickness of the interface layer. The influence of the GR height h_{gx} within the embankment is studied using a 7.2-m high embankment and a pile network spacing of s = 2.0m.

Fig. 7a shows the efficiency for one GR layer at the following altitudes: 0m (like in the models presented in Fig. 6), 0.2, 0.4, 0.8, 1.2 and 1.8m, respectively. The case model without GR is also displayed here for comparison purposes. Both the reference model (i.e., h_{gx} = 0m) and the one with a small altitude (h_{gx} = 0.2m) obtain an efficiency E_F = 100%. However, the efficiency with h_{gx} = 0.2m is lower than in the reference case until the tray displacement $\Delta\omega$ reaches 0.28m. In both cases, the GR has been subjected to irreversible plastic strain (as shown in Fig. 3). In the next tests conducted with increasing geosynthetic altitudes (h_{gx} = 0.4, 0.8, 1.2 and 1.8m), the efficiency is lower than in the reference case (h_{gx} = 0m). Compared with the case without GR, the efficiency is higher for small displacements. For settlement higher than 0.35m, the efficiency is even lower for h_{gx} equal or higher than 0.8m. The reason for that is that the GR "breaks" the arching effect occurring within the embankment. The consequence is that the soil below the GR transmits a load directly to the tray, the value of which is much higher than the stress transferred towards piles. Because of this the efficiency can be even lower than in the case without GR. For h_{gx} = 0.4m, the efficiency increases again for a displacement equal to 0.45m. This is due to the fact that, as soon as the embankment has been sufficiently punched by the pile (i.e., $\Delta\omega$ equal to the geosynthetic level), the tension force in the GR increases and the membrane effect increases. Moreover, the arching effect is produced again above the GR. For $h_{gx} \geq$ 0.4m, the GR strain does not reached plastic yield.

The load transferred towards the piles depends on the stiffness and position of the GR within the embankment. A stiff and basal GR produces higher transfer for low soft soil settlement because of maximum membrane and arching effects. In other words, the GR has no effect in terms of load transfer if it is placed too high within the embankment. In this case, indeed, load transfer is even lower than the value achieved for the same embankment without GR.

4.4.*Surcharge applied on the embankment*

4.4.1. *Water tank*

Until now only load transfers due to the embankment weight itself have been considered. In this section, we examine how an external surcharge applied here using a water tank can modify the load transfer efficiency.

Using an additional device, it is possible to apply a surcharge at the top of the embankment to investigate how the load transfer can be affected by a homogeneous and static surcharge (Fig. 8). Two different embankment thicknesses (H = 1.8 m and H = 3.2m) and two surcharge values (40 and 80 kPa) are tested.

Fig. 8 (a) displays the efficiency versus the tray displacement for the case where H is equal to 1.8m. Without GR, the surcharge (40kPa for T20 & 80kPa for T23) improves the load transfer efficiency in comparison with the case where no surcharge is applied (T1). In fact, applying an increased average pressure on the embankment top surface increases effective stress significantly. As a result the arching effect, which is stress dependent, increases. It means that the load transferred towards the piles increases when a hydraulic load is applied on the embankment top. The case of a 3.2-m thick embankment where the intensity of q_0 has less influence than for the case H=1.8m is presented in Fig. 8 (b). The efficiency is increased only for the case q_0 = 80kPa and for displacements larger than 0.2m. For a thicker embankment, the hydraulic stress causes a relatively lower increase in effective stress. Therefore, the same hydraulic load has less influence on the efficiency for H = 3.2m than for H = 1.8m. With a geosynthetic reinforcement, the efficiency is very similar for all cases (no surcharge, q_0 = 40kPa or 80kPa). The decreasing efficiency observed for test T27 and T30 is due to the heterogeneity of the load sensors and provides an underestimated mean load inside the piles. Only the tests without surcharge and with H = 3.2m reveal a small difference. If we consider that, for a GRPSE, the efficiency is due to both arching and membrane effects, applying a stress does not modify the behaviour of the GR, and thus the efficiency value.

The interesting finding of this section is that the water tank by applying a homogeneous stress increases arching significantly, particularly in the case of unreinforced piled embankments. This increase is particularly noticeable in case of thin embankments because they have relatively low stress levels due to their weight. In GRPSE, however, the membrane effect almost entirely conceals the benefits of external loading.

4.4.2. *Nature of the surcharge*

Different loads can be applied on an embankment of constant thickness (here 1.8m). The aim of this section is to compare the embankment behaviour for different model configurations (i.e., different models corresponding to a hydraulic surcharge or a granular additional thickness).

A thin embankment model is then considered (i.e., H/H_{arch} = 1.4 with H = 1.8m) and three different configurations are adopted (Fig. 4):

(i) Thick embankments (7.2m) without surcharge,

(ii) Thin embankments (1.8m) supporting the weight of an additional 5.4m one separated by a PP25 GR,

(iii) Thin embankments (1.8m) with some hydraulic surcharges applied via a soft membrane.

All the configurations are tested for piled embankments without (T10, T17 and T20) and with (T11, T19 and T21) geosynthetic basal reinforcement (PP25: J_a = 4.0 MN/m). For instance, T17 corresponds to an embankment with no basal GR and a PP60 geosynthetic layer (J_a = 16.8MN/m) placed at h_{gx} = 1.8m. T19 corresponds to a 7.2m thick embankment, within which two PP25 geosynthetic layers (J_a = 4 MN/m) are placed (one at basal level and the second at h_{gx} = 1.8m) as schematically shown in Fig. 4b.

For the configurations without basal reinforcement (Fig. 9a), the load transfer increases with the tray displacement and reaches approximately the same value (around 65%). We observe that the surcharge applied using the water tank (test T20) produces a uniform pressure whereas some arching effects appear within the granular thickness above the PP60 geosynthetic (test T17). For the T17 model, the GR is located at a height of 1.8m and presents some higher efficiencies due to the membrane effect. The difference observed between the T17 and T20 curves can be explained by the fact that the total embankment thickness is larger resulting in some additional arching effect. This is also the case when the water surcharge produces an increasing effective stress at the embankment top surface in the case of test T20. As regards arching effect within a thick embankment, the granular thickness is more relevant than the effective stress at its base.

The curves E_F - $\Delta\omega$ of the tests conducted with the basal GR are plotted in Fig. 9(b). The efficiencies are very similar save for the case with a single embankment (T11), for which they are lower. For the two other cases, the 1.8-m thick layer between the basal GR and the membrane/second GR is stressed and may generate some higher load transfer efficiencies.

346 The difference observed between curve T11 and the other curves can be accounted for by test
347 variability.
348 We can then conclude that the load transfer efficiency is slightly higher for thicker
349 embankments because of arching/shearing effects occurring within the whole thickness and
350 not only at the bottom of the embankment (case without GR). As for GRPSE, on the other
351 hand, the impact of the surcharge load type on efficiency is negligible.
352

5. NUMERICAL MODELLING

Physical modelling is combined to numerical calculation to obtain the stress and deformation distributions inside the embankment and on the GR.

5.1. *Definition of the numerical model*

A previous numerical model has been developed by Girout et al. (2014) using the finite element software Plaxis for a two-dimensional (2D) model in an axisymmetrical unit-cell approach (corresponding to one pile of a network situated far from the embankment slope). This study has also demonstrated that a three-dimensional (3D) model is not required in this case because no better fitting with the experimental results is obtained.

5.1.1. Geometry

The equivalent radius R_{eq} of the unit-cell is given by:

$$R_{eq} = \sqrt{s^2/\pi} \tag{3}$$

The mesh is built automatically with 15-nodes elements. Each model contains three distinctive parts as shown in Fig. 10:

(i) the embankment, on which the surcharge load q_0 is applied,

(ii) the pile,

(iii) the tray, at the bottom of which the downward vertical displacement $\Delta\omega$ is applied.

Pile/tray, GR/tray and pile/embankment interactions are modelled using some interfaces. The interface on top of the GR is associated to a material whose characteristics are equal to that of the embankment. The other interface characteristics are found in Girout et al. (2014). The geosynthetic reinforcement is modeled as a beam working under tension only. The beam mean secant stiffness is chosen to model the PP25 GR ($J_a^{(p)}$ = 4000kN/m).

5.1.2. *Constitutive models*

In order to model the embankment behaviour, a hypoplastic model is chosen. This hypoplastic model, indeed, takes the change in the embankment void ratio during the tray downward displacement into account, as showed by Girout et al. (2014). The pile and the tray are modelled considering an elastic law with an infinite stiffness in contrast to the embankment material stiffness.

5.1.3. *Process*

Numerical modelling follows the same process as that for centrifuge testing. The first step consists in numerically applying macro-gravity by increasing earth standard gravity 20 times

(N = 20). Then, the surcharge load is applied. Finally, the tray downward displacement is initiated with a 1-mm step until the GR comes loose from the tray. Additional information is found in Girout et al. (2014).

5.2.*Results*

This study focuses on stress and displacement/deformation distributions within embankments. It is also interesting in pointing up GR displacements and tensile loads, which is impossible with the centrifuge at the scale used (N = 20). The authors have chosen here to discuss the results for the GRPSE case. Two reinforcement layers are considered (one basal and the second at h_{gx} = 0.2m) within a thin embankment (H = 1.0m), on which a hydraulic surcharge (q_0 = 80kPa) is applied and with the same spacing that the centrifuged tests (s = 2.0m). This configuration is compared with a previous case used as the reference case by Girout et al. (2014) in order to investigate how the second GR behaves within the embankment. These configurations have also been experimentally tested using the geotechnical centrifuge and are listed in Table 4 as TA (one GR) and TB (two GR).

Fig. 11 presents the load transfer efficiency for both configurations. The numerical and experimental efficiencies obtained are quite similar, or even lower for the case with two GR. This trend is also observed with the numerical calculation. As observed previously by the authors, the total displacement requires for the GR to come loose from the tray (i.e., $\Delta\omega = \delta_g$) is numerically underestimated.

Fig. 12 shows the distribution of four parameters within the embankment at their final state (i.e., $\Delta\omega$ higher than δ_g): the vertical stress σ_{zz} (Fig. 12a), the vertical displacement U_{zz} (Fig. 12b), the shear stress σ_{rz} (Fig. 12c) and the void ratio e (Fig. 12d). Before the beginning of the tray displacement, the initial vertical stress σ_{ss} is the sum of the embankment column weight plus the hydraulic load, i.e., 95kPa. After the downward displacement, three distinctive areas for the σ_{zz} distribution are noticeable (Fig. 12a): 1) above the pile head (σ_{zz} higher than 600 kPa), 2) above the center between the piles (σ_{zz} lower than 50 kPa) and 3) a transitional area (σ_{zz} value decreasing in intensity but increasing in volume). The σ_{zz} isovalues of the two GR case are similar to the single GR case presented by Girout et al. (2014). Higher stresses are applied on the pile and part of the GR. The installation of the GR increases pile head loading by membrane effect. The embankment column in the half-space between both piles is under-stressed. During the downward displacement, the granular material layer between both GR is compressed, especially above the pile (which is much stiffer than the GR). U_{zz} (Fig. 12b) makes it possible

to locate the second GR layer location with a small lateral displacement of the iso-value at h_{gx} = 0.2m. σ_{rz} (Fig. 12c) shows a similar trend than in the single basal GR case, except that some higher values are obtained above the pile edge because of the stress concentration below the top GR layer. The void ratio distribution (Fig. 12d) also reveals a fragmented shear band (characterized by lower void ratio) because of the presence of the second GR layer. Nevertheless, the other bands occurring above the embankment suggest that arching is well developed.

The tensile load T and the vertical displacement $U_{zz\,g}$ in the GR are displayed in Fig. 13. Considering TB (the 2 GR case), T reaches its maximum value at the pile edge (as shown in Fig. 13a) and decreases until the equivalent radius, R_{eq}. In Fig. 13b U_{zz} is nil above the pile and increases until reaching a maximum value δ_g at $r = R_{eq}$. The basal GR layer shows that the behaviour is very similar to TA (single basal GR). The only difference is a peak at 220kN/m (instead of 230kN/m in the single basal GR case). The second GR (h_{gx} = 0.2m) has a tensile load equal to 65kN/m, which is maximum at the pile center. This value is much lower than the value obtained in the basal GR case. The same observation is made *in situ* as, for example, in Briançon and Simon (2012). The tensile load is reduced when the spacing r exceeds 0.25m (i.e., the pile radius, R_{eq}) reaching its minimum value at the center.

The vertical displacement of the basal GR (Fig. 13 b) is no different from the single GR case except above the pile. Above the pile, indeed, the second GR descends vertically some 0.02m because of the densification of the granular material. Above the tray, the second GR behaves like the basal GR. The second GR also introduces a membrane effect, whose impact on the tests, however, is negligible.

6. CONCLUSIONS

The present study has been conducted to examine the behaviour of a piled embankment system implemented with and without basal geosynthetic reinforcement. 33 tests have been performed using a geotechnical centrifuge to determine the influence of the embankment thickness, the geosynthetic altitude within the embankment, the secant stiffness of the geosynthetic layers and the surcharge applied on the surface.

Different findings are obtained:

(i) The load transferred towards the piles increases with the embankment thickness, in the same way as the load applied on the soft soil. For a 7.2- m high embankment and an area replacement ratio of 4.91%, the maximum load transfer efficiency is equal to 65%. Some arching effects appear within the embankment, the extent of which depends on the prescribed tray displacement.

(ii) The presence of geosynthetic reinforcements enhances the efficiency of load transfer towards the piles. The membrane effect is more noticeable as the prescribed tray displacement increases. For the area replacement ratio studied here (α = 4.91 %) and because of the prescribed settlement of the soft soil, the efficiency reaches 100%. The stiffer the geosynthetic, the lower the deflection.

(iii) The part of the load transferred towards the piles depends on the stiffness and position of the GR within the embankment. A stiff and basal GR generates higher transfers for low soft soil settlements because of maximum membrane and arching effects. Two geosynthetic reinforcement layers are used for the same model geometry. The total vertical displacement of the geosynthetic decreases when its secant stiffness increases. The membrane effect is at the maximum when the geosynthetic layer is located close to the pile top. In order to reduce plastic strain within the geosynthetic, a thin granular layer can be laid under the geosynthetic, which is no thicker than 0.2m. According to the test results, the efficiency is similar for very high soft soil settlement with the geosynthetic layer no thicker than 0.2m.

(iv) Considering the results available (embankment thicknesses of 1.8m and 3.2m, respectively, area replacement ratio of 4.91%, surcharge of 40 and 80 kPa), applying a temporary surcharge results in some quite different load transfer efficiencies for thinner embankments. The main finding here is that the water tank exerts a homogeneous stress. Consequently, arching, which is stress dependent, is significantly increased and improves the efficiency. Improvement is limited in the case of thick embankments

because of a relatively lower increase in the effective stress. GRPSE is largely unaffected because of an additional load transfer at the embankment bottom due to the membrane effect.

(v) Considering the same average stress applied at the bottom of pile-supported embankments, the key feature as regards load transfer is arching, which can be improved by applying an external surcharge. As for GRPSE, arching and external surcharge have similar effects.

(vi) Numerical modelling demonstrates that the addition of a second GR within embankments does not enhance GR deflection reduction. Although the presence of a second GR layer breaks the arching mechanisms at the bottom, it, however, does not stop these mechanisms in the embankment areas situated above this GR and even enhances load transfer through its membrane effect.

NOTATION

Basic SI units are shown in parentheses.

A	Load transferred towards the pile by arching effect (N)
B	Load transferred towards the pile by membrane effect (N)
C_U	Uniformity coefficient
C_C	Coefficient of gradation
d	Pile diameter (m)
d_{50}	Diameter of 50% passing
E_F	Load transfer efficiency defined in Equation (1) (%)
e	Void ratio of the embankment material
F_m	Mean load transferred toward the rigid pile network (N)
g	Standard earth acceleration ($m.s^{-2}$)
H	Embankment thickness (m)
H_{arch}	Radius of the arching effect for the analytical calculation defined in Equation (2) (m)
h_{gx}	Altitude of the geosynthetic layer inside the embankment (m)
J_a	Average Secant stiffness for the geosynthetic reinforcement (N/m)
q_0	Surcharge applied via the water tank (Pa)
N	Scale factor
R_{eq}	Equivalent radius in numerical modelling (m) defined in Equation (3)
r	Radial spacing from pile axis in axisymmetrical configuration (m)
s	Spacing between pile-axis (m)
$T_{(max)}$	(Maximum) tensile load of the geosynthetic (N/m)
U_{zz}	Numerically obtained vertical displacement in the embankment (m)
$U_{zz\,g}$	Numerically obtained vertical displacement in the geogrid (m)
z	Height within embankment (m)
$X^{(m)/(p)}$	Parameter X given at model/prototype scale
α	Area replacement ratio of the pile network (%)
$\varepsilon_{g\,max}$	Geosynthetic deformation at T_{max} (%)
$\Delta\omega_{(max)}$	(Maximum)Tray displacement in its center (m)
δ_g	Deflection of the geosynthetic layer (m)
ϕ_p	Friction angle of the Hostun sand mix (°)
ρ_d	Embankment density (kg/m^3)
ρ_s	Volumic mass of solids (kg/m^3)

515 σ_{zz} Vertical stress (Pa)

516 σ_{rz} Shear stress (Pa)

517 γ_d Embankment unit weight (N/m^3)

518

ABREVIATION

GR Geosynthetic Reinforcement

GRPSE Geosynthetic-Reinforced Pile-Supported Embankment

MT Mobile Tray

PP25 Polypropylene Woven Geotextile with T = 25 kN/m

PP60 Polypropylene Woven Geotextile with 62 kN/m < T < 66 kN/m

526 **REFERENCES**

527 Bhasi, A. & Rajagopal, K. (2014). Geosynthetic-Reinforced Piled Embankments: Comparison
528 of Numerical and Analytical Methods. *International Journal of Geomechanics*, 15(5):1-
529 12.

530 Blanc, M., Rault, G., Thorel, L. & Almeida, M.S.S. (2013). Centrifuge investigation of load
531 transfer mechanisms in a granular mattress above a rigid inclusions network. *Geotextiles*
532 *and Geomembranes*, 36 (0), 92–105.

533 Blanc, M., Thorel, L., Girout, R. & Almeida, M. (2014). Geosynthetic reinforcement of a
534 granular load transfer platform above rigid inclusions: comparison between centrifuge
535 testing and analytical modelling. *Geosynthetics International*, 21 (1), 37–52.

536 Briançon, L. & Simon, B. (2012). Performance of Pile-Supported Embankment over Soft Soil:
537 Full-Scale Experiment. *Journal of Geotechnical and Geoenvironmental Engineering* 138
538 (4), 551–561.

539 Briançon L. & Dias D. (2015). Monitoring and numerical investigation of rigid inclusions
540 reinforced industrial building, *Canadian Geotechnical Journal*. 52 (10), 1592-1604

541 Briançon, L. & B. Simon. (2017) "Pile-Supported Embankment over Soft Soil for a High-Speed
542 Line." *Geosynthetics International*, 1–13.

543 Chen, R. P., Wang, Y. W. , Ye, X. W., Bian, X. C. Dong, X. P. (2016). Tensile Force of
544 Geogrids Embedded in Pile-Supported Reinforced Embankment: A Full-Scale
545 Experimental Study. *Geotextiles and Geomembranes*, 44 (2): 157–169.

546 EBGEO (2011). Recommendations for Design and Analysis of Earth Structures using
547 Geosynthetic Reinforcements - *EBGEO, Deutsche Gesellschaft fr Geotechnik* e V. /
548 German Geotechnical. John Wiley & Sons. Berlin, Germany, 2011, 361p

549 Ellis, E. & Aslam, R., (2009). Arching in piled embankments: comparison of centrifuge tests
550 and predictive methods - part 2 of 2. *Ground Engineering*, 42 (0):34–38.

551 Eskişar, T., Otani, J. & Hironaka, J. (2012). Visualization of soil arching on reinforced
552 embankment with rigid pile foundation using X-ray CT. *Geotextiles and Geomembranes*,
553 32: 44–54.

554 Fagundes, D., Almeida, M.S.S., Girout, R., Blanc, M. &Thorel, L. (2015). Behaviour of piled
555 embankment without reinforcement''. *Proceedings of the Institution of Civil Engineers -*
556 *Geotechnical Engineering*, 168(6): 1-12.

557 Fagundes D., Almeida M., Thorel L., Blanc M. (2017) Load transfer mechanism and
558 deformation of reinforced piled embankments. *Geotextiles and Geomembranes* 45 (2):1-
559 10,
560 Garnier, J., Gaudin, C., Springman, S.M., Culligan, P.J., Goodings, D.J., Konig, D., Kutter,
561 B.L., Phillips, R., Randolph, M.F. & Thorel, L. (2007). Catalogue of scaling laws and
562 similitude questions in geotechnical centrifuge modelling. *International Journal of*
563 *Physical Modelling in Geotechnics*, 17(3): 1–24.
564 Girout, R., Blanc, M., Thorel, L, Fagundes, D. F. & Almeida, M. (2016). Arching and
565 deformation in a piled embankment: centrifuge tests compared to analytical calculations.
566 *Journal of Geotechnical and Geoenvironmental Engineering,* 142 (12):1-10.
567 Girout, R., (2014). Prise en compte des géosynthétiques dans les mécanismes de transfert de
568 charge d'un matelas granulaire renforcés par inclusions rigides: Modélisation physique et
569 numérique. Thèse de doctorat, Ecole Centrale de Nantes, 300p (in French)
570 Girout, R., Blanc, M., Dias, D. & Thorel, L. (2014). Numerical analysis of a geosynthetic-
571 reinforced piled load transfer platform – Validation on centrifuge test. *Geotextiles and*
572 *Geomembranes* 42 (5): 525–539.
573 Han-Jiang, L., Zhen, J.-J., Zhang, J., Zhang, R.-J. & Cui, L. (2014). DEM analysis of soil -
574 arching within geogrid -reinforced and unreinforced pile-supported embankments.
575 *Computer and Geotechnics*, 61(0): 13–23.
576 Hewlett, W. & Randolph, M.A. (1988). Analysis of piled embankments. *Ground Engineering*
577 (21): 12–18.
578 IREX (2012). Recommendations for the Design Construction and Control of Rigid Inclusion
579 Ground Improvements. ASIRi, Presses Des Ponts. Paris. 384p.
580 Jenck O., Dias, D. & Kastner R. (2005). Soft Ground improvement by vertical rigid piles-Two-
581 dimensional physical modelling and comparison with current design methods. *Soils and*
582 *Foundation,* 45 (6): 15-31.
583 Jenck O., Dias D. & Kastner R. (2007). Two-dimensional physical and numerical modelling of
584 a pile supported earth platform over soft soil, *Journal of Geotechnical and*
585 *Geoenvironmental Engineering*, ASCE, 133 (3) :295-305.
586 King, D. J., Bouazza, A., Gniel, J.R., Rowe, K. R. & Bui, H. H.. (2017). Serviceability Design
587 for Geosynthetic Reinforced Column Supported Embankments. *Geotextiles and*
588 *Geomembranes*:1-19.

589 Le Hello, B. (2007). Renforcement par géosynthetiques des remblais sur inclusions rigides,
590 étude expérimentale en vraie grandeur et analyse numérique. Thèse de doctorat,
591 l'université Grenoble I, 234p (in French).
592 Le Hello, B. & Villard, P. (2009). Embankments reinforced by piles and geosynthetics –
593 Numerical and experimental studies with the transfer of load on the soil embankment.
594 *Engineering Geology*, 106: 78 – 91.
595 Nunez, M., Briançon, L. & Dias, D. (2013). Analyses of a pile-supported embankment over
596 soft clay: Full-scale experiment, analytical and numerical approaches, *Engineering*
597 *Geology.*153: 53-67
598 Okyay, U., Dias, D., Thorel, L. & Rault, G. (2014). Centrifuge Modelling of a Pile-Supported
599 Granular Earth-Platform. *Journal of Geotechnical and Geoenvironmental Engineering*,
600 140 (2): 1-12.
601 Okyay, U. (2010). Etude expérimentale et numérique des transferts de charge dans un massif
602 renforcé par inclusions rigides. Applications à des cas de chargements statiques et
603 dynamiques. Thèse de Docteur ès Sciences, Institut National des Sciences Appliquées,
604 Univ. of Lyon, Lyon, France 402 p. (in French)
605 Rault, G., Thorel, L., Néel, A., Buttigieg, S., Derkx, F., Six, G., & Okyay, U. (2010). Mobile
606 Tray for Simulation of 3D Load Transfer in Pile-Supported Earth Platforms. Laue,
607 Sewards, (Editor) *Physical modelling in Geotechnics*. Vol 2. Proceedings of a symposium
608 held in Zurich, Switzerland, 28th June- 1st July 2010, pp 261-266.
609 Van Eekelen, S.J.M., Bezuijen, A. & van Tol, A.F. (2015). Validation of analytical models for
610 the design of basal reinforced piled embankments. *Geotextiles and Geomembranes*, 43 (1):
611 56-81
612 Van Eekelen, S. J. M., Bezuijen, A., Lodder, H. J. & van Tol., A. F. (2012a). Model
613 Experiments on Piled Embankments. Part I. *Geotextiles and Geomembranes* 32: 69–81.
614 Van Eekelen, S. J. M., Bezuijen, A., Lodder, H. J. & van Tol., A. F. (2012b). Model
615 Experiments on Piled Embankments. Part II. *Geotextiles and Geomembranes* 32: 82–94.
616 Villard, P. &, Giraud, H. (1998). Three-Dimensional Modelling of the Behaviour of Geotextile
617 Sheets as Membranes. *Textile Research Journal* 68, 11: 797–806.
618 Xing, H., Zhang, Z., Liu, H. & Wei, H. (2014). Large-scale tests of pile-supported earth
619 platform with and without geogrid. *Geotextiles and Geomembranes*, 42 (6): 586–598.

620 Zhuang, Y. & Wang, K.Y. (2015). Three-Dimensional Behaviour of Biaxial Geogrid in a Piled
621 Embankment: Numerical Investigation. *Canadian Geotechnical Journal* 52 (10):1629-
622 1635.
623 Zhuang, Y. & Wang, K.Y. (2016). Finite-Element Analysis on the Effect of Subsoil in
624 Reinforced Piled Embankments and Comparison with Theoretical Method Predictions.
625 *International Journal of Geomechanics*, 16 (5): 1–15.
626 Zhuang, Y., & Ellis, E. A. (2016). Finite-Element Analysis of a Piled Embankment with
627 Reinforcement and Subsoil. *Géotechnique* 66 (7): 596–601.
628
629

665 **TABLES**

666 **Table 1 Scaling factors**

	Prototype	Small-scale model
Force (N)	1	$1/N^2$
Stress (Pa)	1	1
Deformation (%)	1	1
Length (m)	1	$1/N$
Secant stiffness (N/m)	1	$1/N$

667

668

669

670 **Table 2 Characteristics of the mix Hostun sand (γ_d = 15.8 kN/m^3 and ϕ_p = 38°)**

d_{50} (mm)	C_U	C_C	$\rho_{d\,min}$ (g/cm^3)	$\rho_{d\,max}$ (g/cm^3)	ρ_s (g/cm^3)
0.32	3.52	0.88	1.40	1.73	2.65

671

672

673

674 **Table 3 Properties of the geosynthetic reinforcement on prototype scale**

Geosynthetic	PP25		PP60	
	Cross	Machine	Cross	Machine
T_{max} (kN/m)	478	490	1320	1240
J_a (MN/m)	4.76	2.96	16.8	16.8
ε_{gmax} (%) for $T = T_{max}$	12.9	19.3	9	9

675

676 **Table 4 List of the experimental test campaign (s = 2.0 m, d = 0.5 m, H_{arch} = 1.2m (as defined in**

677 **Equation (2), α = 4.91 %, ρ_d = 1.62kg/m^3)**

Tests (TX)	H (m)	H/H_{arch}	J_a (MN/m)	h_{gx} (m)	q_0 (kPa)
TA/TB	1.0	0.78	4	0/0;0.2	80
T1/T2/T3	1.8	1.5	-/4/16.8	0	0
T4/T5/T6	3.2	2.7	-/4/16.8	0	0
T7/T8/T9	5	4.3	-/4/16.8	0	0
T10/T11/T12	7.2	6.2	-/4/16.8	0	0
T13/T14/T15/T16/T17	7.2	6.2	16.8	0.2/0.4/0.8/1.2/1.8	0
T18 /T19$^{(2\ PP25\ GR)}$	7.2	6.2	4	1.8 / 0;1.8	0
T20/T21/T22	1.8	1.5	-/4/16.8	0	80
T23/T24/T25	1.8	1.5	-/4/16.8	0	40
T26/T27/T28	3.2	2.75	-/4/16.8	0	40
T29/T30/T31	3.2	2.75	-/4/16.8	0	80

678

679

680 **FIGURES**

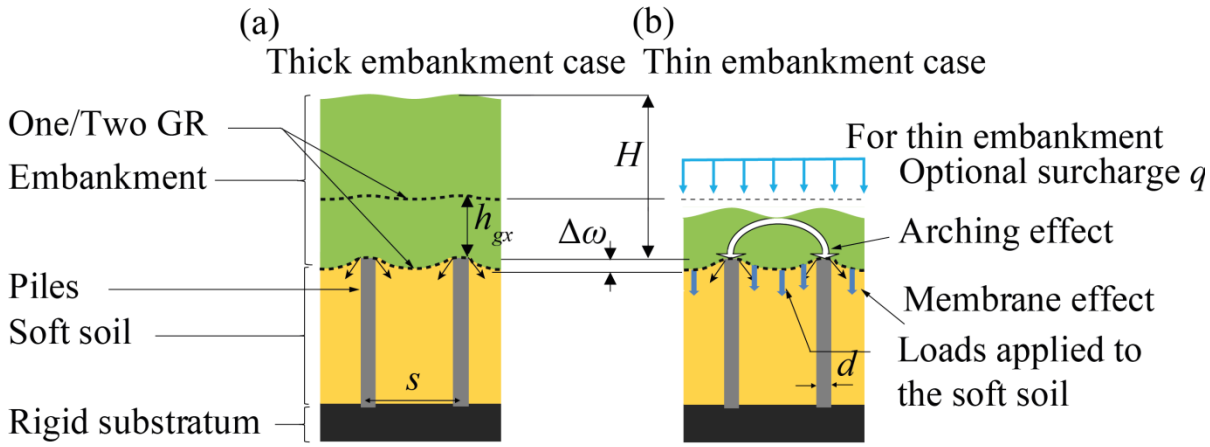

681

682 **Fig. 1 (a) General configuration of a piled embankment reinforced with one/two geosynthetic**
683 **layers (b) Mobilisation of the geosynthetic strength during soft soil settlement**
684

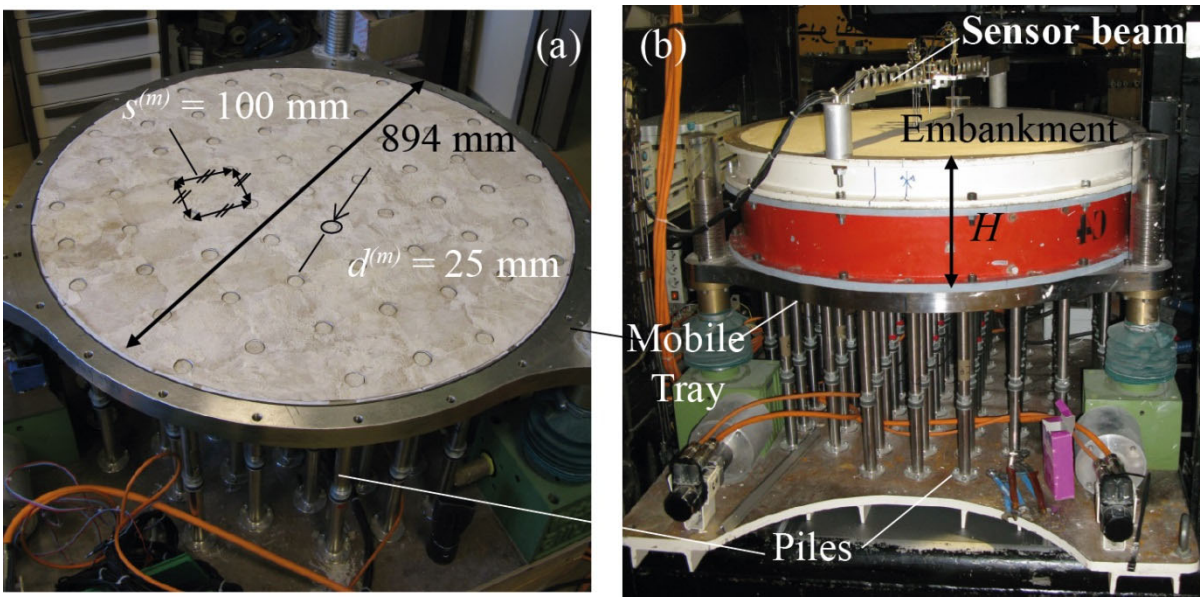

685 **Fig. 2 Mobile Tray Device (a) Surface of the tray and square pile network with a pile diameter**
686 **equal to 25 mm (b) Mobile Tray with model embankment in the centrifuge swinging basket**
687
688

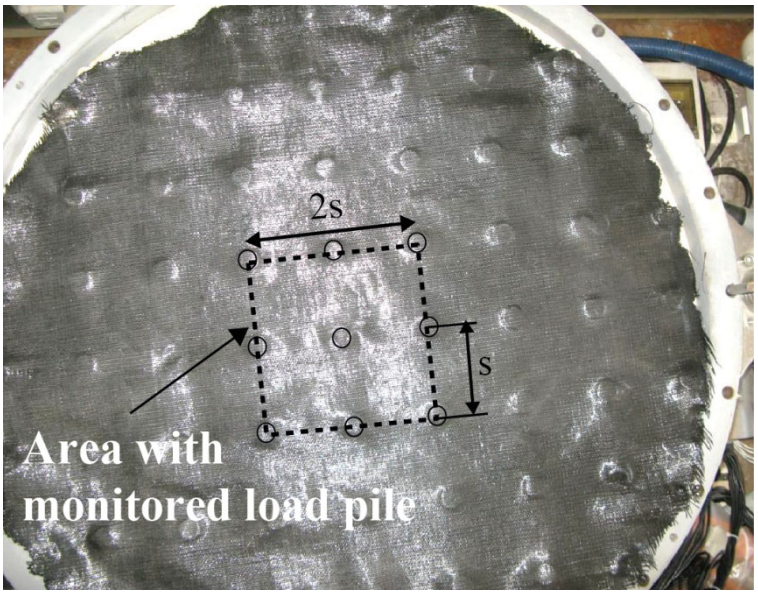

689 **Fig. 3 Geosynthetic layer after testing: localization of the geosynthetic deformations (h_{gx} = 0m and**

690 **$H^{(p)}$ = 7.2m)**

691

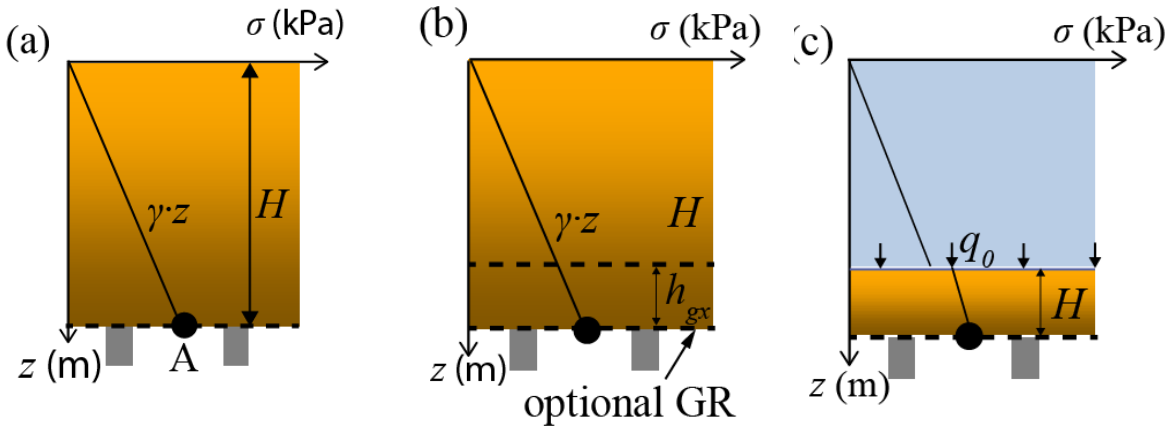

692 **Fig. 4 Geometry of the models in the swinging basket of the centrifuge (a) Single embankment**
693 **(b) Embankment reinforced at $z = H - h_{gx}$ and (c) (Dry) embankment loaded by means of**
694 **hydraulic surcharge**
695

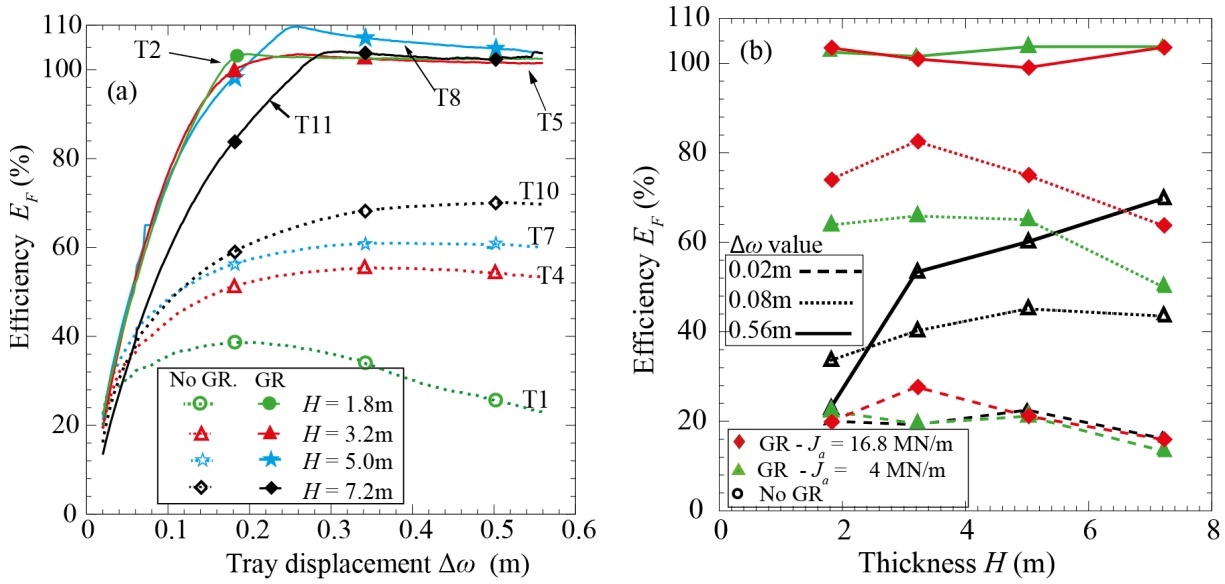

696 **Fig. 5 Efficiency of the load transfer (for H = 1.8 m, H = 3.2 m, H = 5.0m and H = 7.2 m): (a)**
697 **with and without geosynthetic (J_a = 4MN/m) (b) Variations of the efficiency versus H for**
698 **different $\Delta\omega$**
699

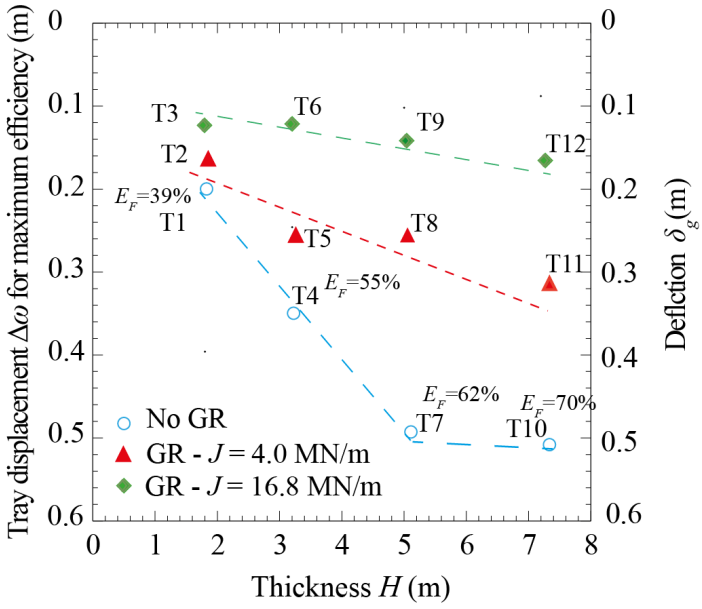

700 **Fig. 6 Tray displacement for the maximum efficiency reached (non-reinforced case) and**
701 **deflection δ_g of both geosynthetic layers (J_a = 4.0 MN/m and 16.8 MN/m) versus thickness *H***
702

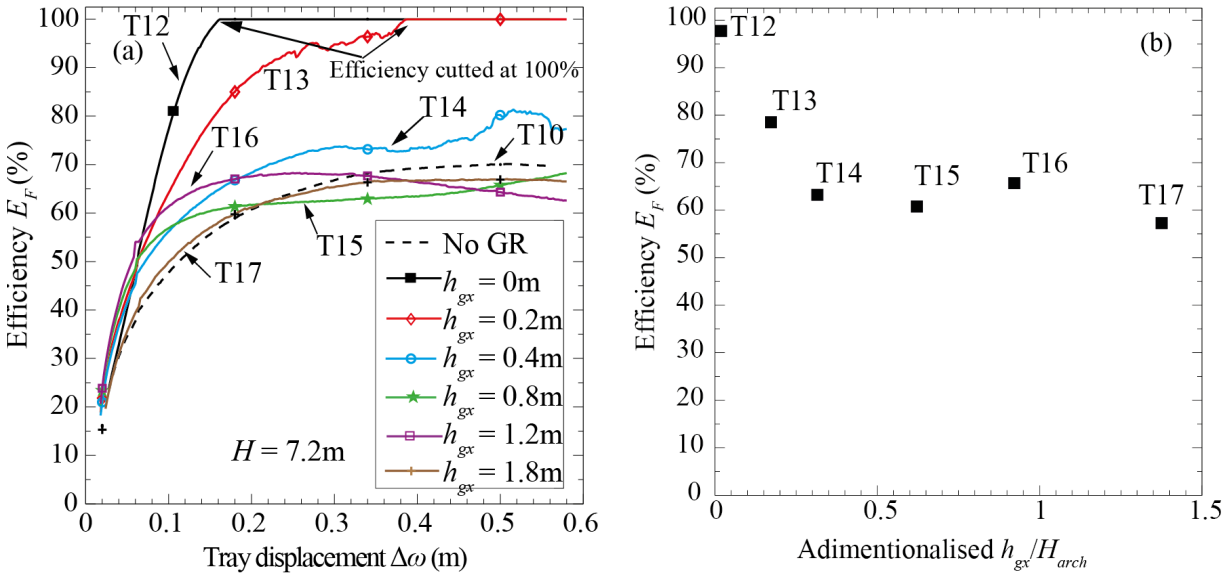

703 **Fig. 7 Influence of the GR for different elevations (a) Efficiency versus tray displacement (b)**
704 **Efficiency versus adimentionalized geosynthetic elevation**
705

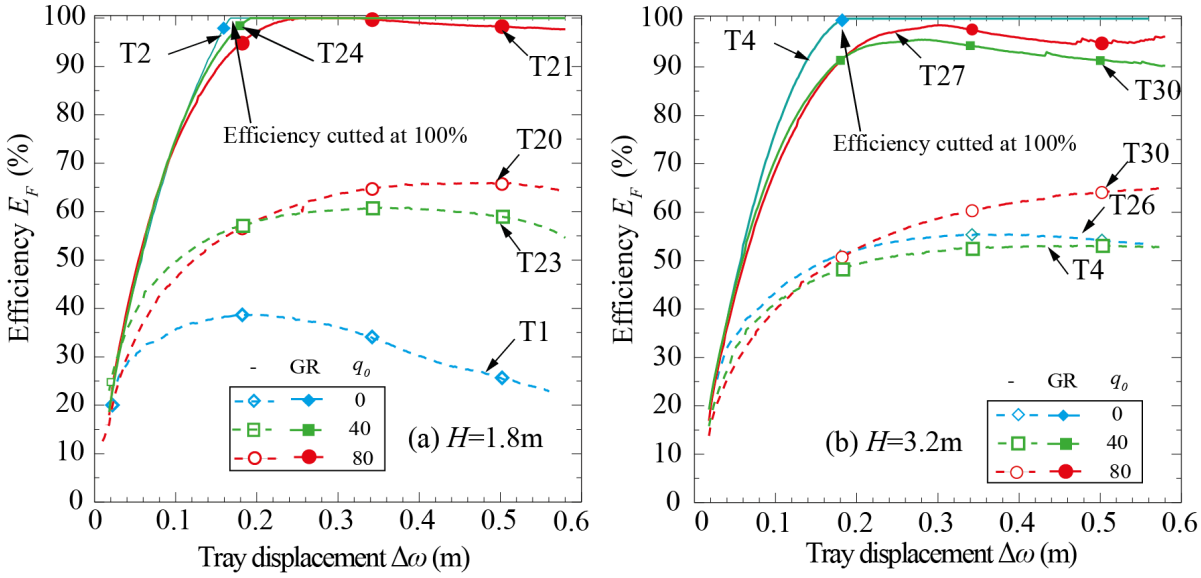

706 **Fig. 8 Influence of the surcharge (q_0 = 0; 40 and 80 kPa): testing with and without geosynthetic**
707 **(a) H = 1.8 m (b) H = 3.2 m**

708
709

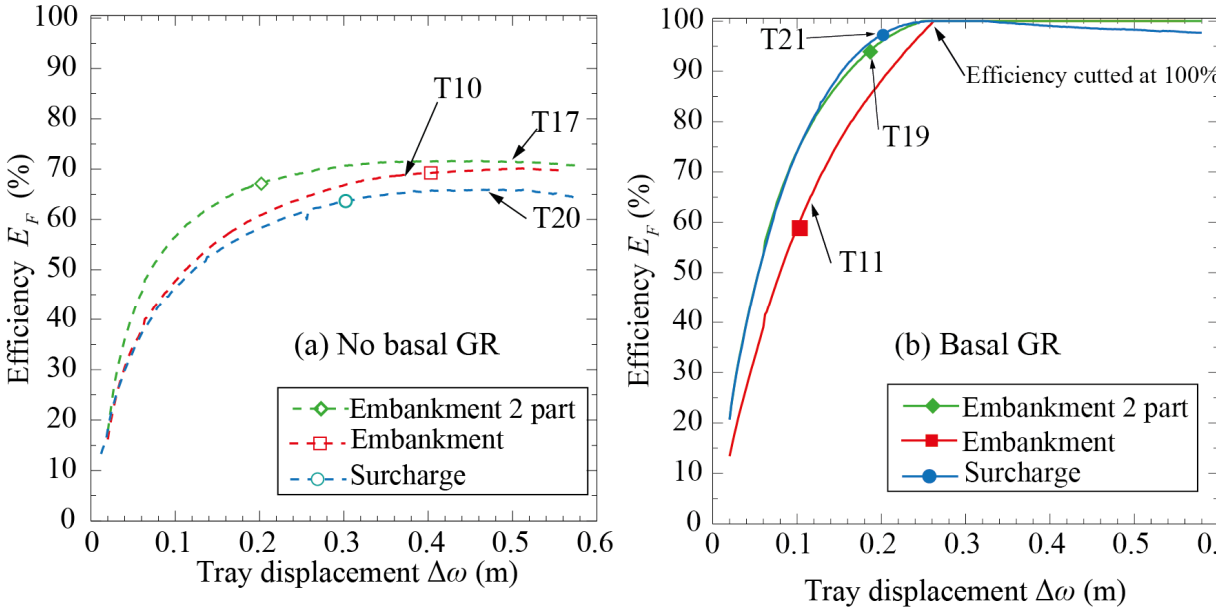

710 **Fig. 9 Comparison of the different types of surcharge applied above the geosynthetic: (a)**
711 **Without basal reinforcement and (b) With basal reinforcement (h_{gx} = 0 m)**
712

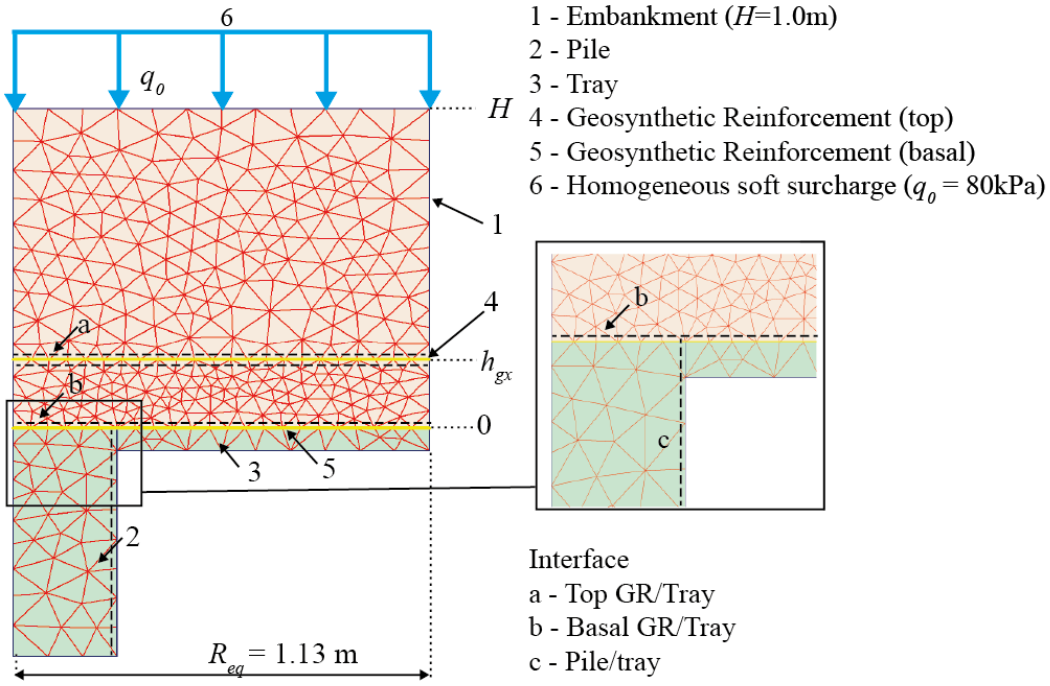

713 **Fig. 10 Definition of the numerical model**

714

715

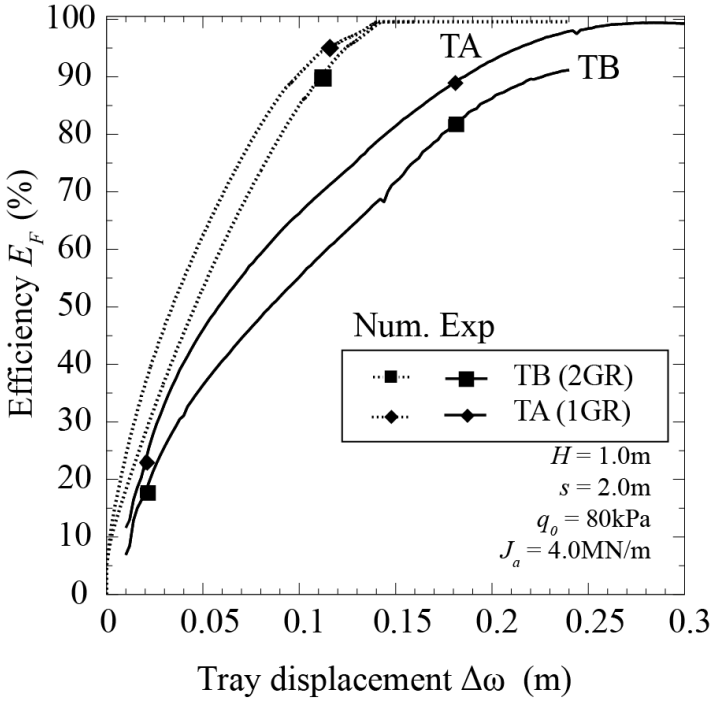

716 **Fig. 11 Load transfer efficiency for GRPSE with one and two GR layers (numerical and physical**

717 **modelling)**

718

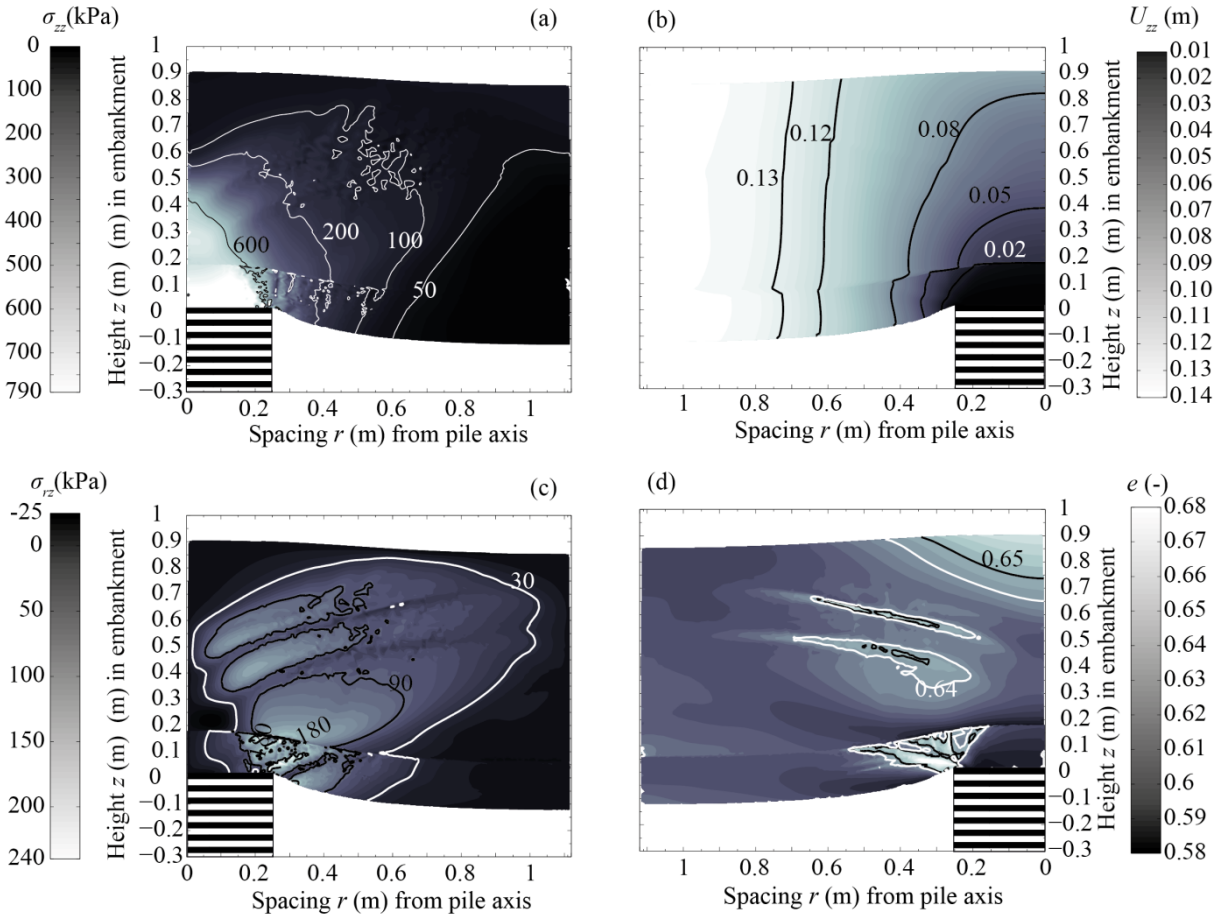

719 **Fig. 12 Finite element modelling of a GRPSE with two GR (h_{gx} = 0 and 0.2m with J_a = 4.0MN/m),**

720 **s = 2.0m, H = 1.0m and q_0 = 80 kPa**

721

722

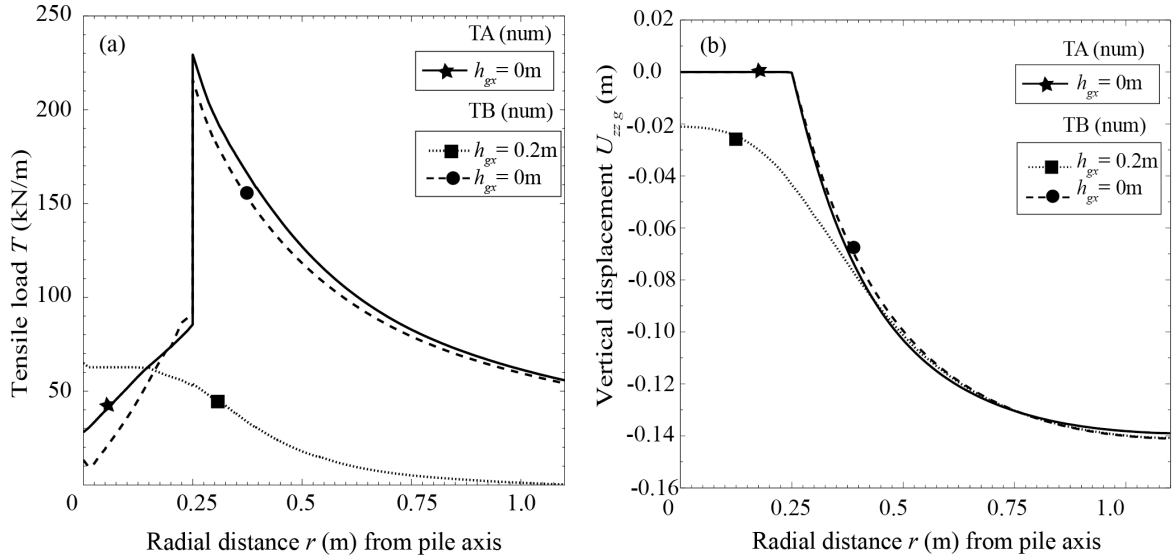

723 **Fig. 13 Distributions for the single basal GR layer case and for the two GR case: (a) tensile load**

724 ***T* and (b) vertical displacement $U_{zz\,g}$**